American Journal of Materials Synthesis and Processing
2017; 2(2): 28-31
http://www.sciencepublishinggroup.com/j/ajmsp
doi: 10.11648/j.ajmsp.20170202.13

Nanophosphors with Partially Polymerized SiO_4 Tetrahedra Produced by Evaporation of $Ca_2Y_8(SiO_4)_6O_2$: Eu Polycrystals

Mikhail Georgievich Zuev[1], Vladislav Genrikhovich Il'ves[2, 3], Sergey Yurievich Sokovnin[2, 3], Elena Yuryevna Zhuravleva[2]

[1]Institute of Solid State Chemistry, Ural Branch of Russian Academy of Sciences, Ekaterinburg, Russia

[2]Ural Federal University Named After First President of Russia B. N. Yeltsin, Ekaterinburg, Russia

[3]Institute of Electrophysics, Ural Branch of Russian Academy of Sciences, Ekaterinburg, Russia

Email address:

zuev@ihim.uran.ru (M. G. Zuev)

To cite this article:

Mikhail Georgievich Zuev, Vladislav Genrikhovich Il'ves, Sergey Yurievich Sokovnin, Elena Yuryevna Zhuravleva. Nanophosphors with Partially Polymerized SiO_4 Tetrahedra Produced by Evaporation of $Ca_2Y_8(SiO_4)_6O_2$: Eu Polycrystals. *American Journal of Materials Synthesis and Processing*. Vol. 2, No. 2, 2017, pp. 28-31. doi: 10.11648/j.ajmsp.20170202.13

Received: June 24, 2016; **Accepted**: April 14, 2017; **Published**: April 27, 2017

Abstract: Nanophosphors in the amorphous state were produced for the first time by pulsed electron beam evaporation of micrometer-sized polycrystalline phosphors of the composition $Ca_2Y_8(SiO_4)_6O_2$: Eu. It was found that the Raman spectrum is modified and the forbidden band width of the samples increases when the particle size lowers from micro- to nanodimensional state. The spectral luminescent characteristics in polycrystalline and amorphous states have been examined. It was established that during the transition to nanoamorphous state the phosphors change their photoluminescence color from red-orange (Eu^{3+}) to blue (Eu^{2+}).

Keywords: Nanophosphor, Microscopy, Raman Spectra, luminescence, Eu^{3+}, Eu^{2+}

1. Introduction

The processes of formation of nanophosphors and the study of the nature of their luminescence represent a topical problem. Of interest is the effect of nanodimensional state of phosphors on radiationless losses and luminescence yield, on broadening and displacement of bands, on the variation in the structure of optical centers, as well as on vibrational spectra. Silicates with oxyapatite structure are known as effective matrices for luminescent materials if they are activated with RE ions [1-8]. There is no information in the literature about the production of nanophosphors based on silicates of the composition $Ca_2Y_8(SiO_4)_6O$: Eu in amorphous state*. It is known that nanophosphors can find application in nanophotonics [9, 10]. New nanophosphor can be used as components to create white LEDs.

In this work, using electron beam evaporation (EBE) of polycrystalline phosphor $Ca_2Y_8(SiO_4)_6O$: Eu targets, we were the first to produce nanopowders (NP) in the amorphous state. A modification of the Raman spectra was found when the particle size decreased from the bulk to the nanodimensional state. Along with isolated SiO_4 groups, a small condensation of SiO_4 tetrahedra occurs in nanoamorphous samples, which is analogous to the polymerization effect in rapid-quenched silicate melts. Their spectral luminescent characteristics have been studied. It was established that during the transition to nanoamorphous state the phosphors change their photoluminescence color from red-orange (Eu^{3+}) to blue (Eu^{2+}).

2. Materials and Methods

In order to obtain NP, we first synthesized $Ca_2Y_{6.4}Eu_{1.6}Si_6O_{26-\delta}$ compounds (δ – nonstoichiometry) with oxyapatitie structure. The samples were synthesized by annealing of a mixture of reagents $CaCO_3$, Y_2O_3, Eu_2O_3, and SiO_2 (at least 99.99% purity grade) in air. Stoichiometric amounts of the initial components were mixed in an agate mortar with addition of ethanol. Then the powders were placed into alundum crucibles and annealed in air in the

temperature interval 1000 – 1450°C with intermediate grinding of the charge. The total time of annealing was 100 h. The XPA was carried out on a Shimadzu XRD-7000 diffractometer (CuK_α radiation, CM-3121 counter monochromator, Scintillation Counter detector) using the ICDD card-file. The X-ray diffraction patterns of the produced samples recorded in the angle interval 2θ = 5 - 70° were refined by the full-profile Rietveld method with the use of the ICDD card-file. Figure 1 shows typical X-ray diffraction patterns of the synthesized solid solutions $Ca_2Y_{6.4}Eu_{1.6}(SiO_4)_6O_2$. The solid solutions belong to the structural type of oxyapatite. These compositions were chosen because in the series of $Ca_2Y_{8(1-x)}Eu_{8x}(SiO_4)_6O_2$ phosphors the solid solution with x = 0.2 has the maximal integral luminescence intensity of Eu^{3+} ions. At x > 0.2, concentration quenching of Eu^{3+} luminescence is observed. The lattice parameters of the $Ca_2Y_{6.4}Eu_{1.6}Si_6O_{26-\delta}$ compound were a = 9.34719, c = 6.78283 Å, and V = 513.220 Å^3.

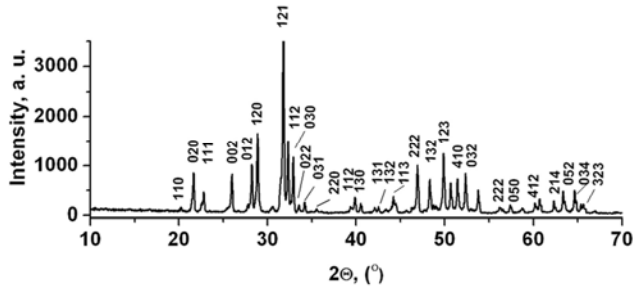

Figure 1. *The X-ray diffraction patterns of $Ca_2Y_{6.4}Eu_{1.6}Si_6O_{26-\delta}$.*

The nanopowders were produced in vacuum by EBE of ceramic targets obtained from $Ca_2Y_{6.4}Eu_{1.6}Si_6O_{26-\delta}$ on a NANOBIM-2 facility [11]. The targets in the form of disks with 20–30 mm diameter and height to 20 mm made of bulk phosphors were produced by annealing of disks at 1400ºC for 40 h. The energy of electrons was 40 keV, the electron beam pulse energy was 1.8 J, the pulse duration was 100 μs, and the pulse frequency was 100–200 Hz. The duration of target evaporation was 40–60 min. The target rotation rate was 8.3 rev/min. The nanopowders were deposited on 4 mm thick noncooled glass substrates placed around the target. The nanopowders were collected from the glass substrates with the use of titanium foil.

The specific surface area of the powders (S_{sp}) was determined by the Brunauer-Emmett-Teller (BET) method [12] on a Micromeritics TriStar 3000 device. The microscopic analysis of the NP was carried out a JEOL JEM 2100 transmission electron microscope. The thermal analysis of the NP was performed on a NETZSCH STA-409 thermal analyzer using TG and DSC methods. The Raman spectra were measured on a Renishaw spectrometer ($\Delta\nu$ = 1000 cm^{-1}) using an argon laser (λ= 514.5 nm) as an excitation source. The photoluminescence and excitation spectra were recorded respectively on an MDR-204 spectrometer (D lamp, R928 photomultiplier from Hamamatsu) and a Cary Eclipse fluorescence spectrophotometer (Xe pulse lamp with exceptionally long lifetime, pulsed at 80 Hz, pulse width at half peak height ~ 2 μs, peak power equivalent to 75 kW). For the experimental estimation of the forbidden band width, the absorption spectra were recorded on a UV-2401 PC device (Shimadzu).

3. Results and Discussion

The powders had a white color. The average particle size of the NP was estimated using the method BET and determined from the HR-TEM results. The characteristics of the BET surface and the properties of the nanoparticles are as follows: S_{sp} (BET) = 232.25 m^2/g, ρ = 4.5 g/cm^3, $d_{BET} \approx$ 5.7 nm. According to the HR-TEM data, $d_{HR\text{-}TEM}$ = 15−18 nm. The microscopy and electronography data show that the NP are practically amorphous (JEOL JEM 2100 microscope). Figure 2 displays the TEM pictures of the NP produced on the basis of $Ca_2Y_{6.4}Eu_{1.6}Si_6O_{26-\delta}$. According to the XPA data, the NP are X-ray amorphous. Synchronous DSC-TG analysis (heating) of the nanoparticles was carried out to determine the NP crystallization temperature (T_{cr}). Crystallization of amorphous nanoparticles begins at a low temperature as indicated by a strong exothermic peak in the temperature interval from 330 to 1000ºC. The low thermal stability of the NP (the initial crystallization temperature is T_{cr} = 330ºC) is caused by the effect of the nanoparticle size factor. The large extent of the exothermic peak is indicative of a slow kinetics of amorphous NP transformation into crystalline powder, which is most likely to be due to different granulometric composition of amorphous nanoparticles.

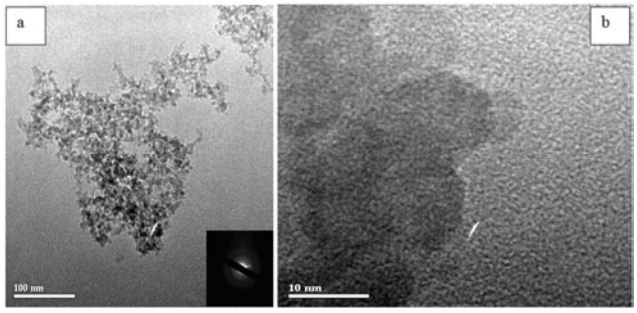

Figure 2. *The TEM images of the NP at different magnifications: (the inset in figure 1,a shows an electron diffraction pattern of amorphous NP); 1,b – quasispherical amorphous nanoparticles.*

The Raman spectra of the $Ca_2Y_{6.4}Eu_{1.6}Si_6O_{26-\delta}$ micropowder and NP were studied (figure 3). In the oxyapatite crystals (sp. gr. P6$_3$/m, Z = 1), the site-symmetry of atoms was Y1 – 4*f*, Ca – 4*f*, Y2 – 6*h*, Si – 6*h*, O – 6*h*, O – 6*h*, O – 12*i*, O – 2*a*; Z = 1. As a result of group-theoretic analysis, the following representation was obtained for the optical vibrations of silicate (1) [13]:

$$\Gamma_{Ca2Y8(SiO4)6O2} = 12A_g\,(R) + 8E_{1g}\,(R) + 13E_{2g}\,(R) + 8A_u\,(IR) + 12E_{1u}\,(IR). \quad (1)$$

Thus, 33 lines should be expected in the Raman spectra, and 20 bands in the IR spectra. The vibrational spectrum of real crystals of $Ca_2Y_8(SiO_4)_6O_2$: Eu can differ from the

spectrum of ideal crystals. This difference can be due to the presence of defects in the crystal lattice. Europium substituting for yttrium atoms may also occupy the 4f and 6h sites. The Raman spectrum of real crystals containing europium impurity and of NP may differ from that of ideal crystals. This difference may be due to the presence of structural defects.

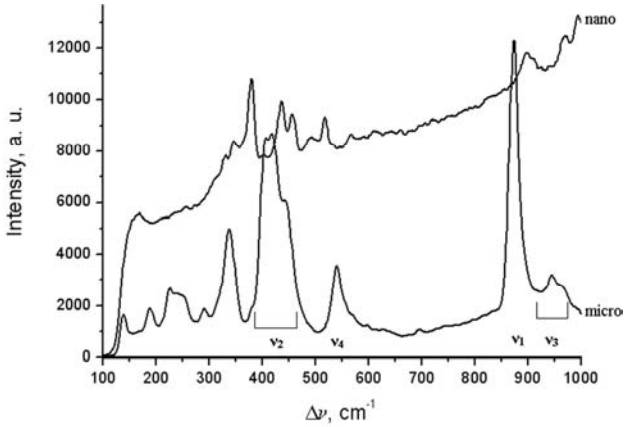

Figure 3. *The Raman spectra of micro- and NP.*

The frequencies ν_1, ν_2, ν_3, and ν_4 of the inner vibrations of isolated tetrahedra SiO_4 are denoted. The spectrum of amorphous NP demonstrates the formation of a structure that differs slightly from that of the initial polycrystalline sample. The arrangement of lines in the NP spectrum indicates that it contains mainly isolated groups SiO_4. At the same time, the appearance of frequencies in the region 600 – 700 cm^{-1} testifies to the formation of an insignificant concentration of polymerized silicon-oxygen fragments in the sample [14]. The displacement of the lines in the interval 290 – 350 cm^{-1} into the high-frequency region is presumably due to the increase in the force coefficient value of component E_{2g} of the libration vibration of the SiO_4 complex. The frequencies ν_2, ν_1, and ν_3 are also shifted into the high-energy region. The frequency ν_4, on the contrary, is shifted into the low-frequency region. These effects in the spectrum can be induced by the unification of a large number of oxygen vacancies in the sample that appear during evaporation of microsamples. The unification of vacancies leads to translation symmetry breakdown. Such symmetry breakdown can be also the cause of line strength reduction at ν_1 [15, 16].

The fundamental absorption spectra of the samples have been recorded. The forbidden band value was found to increase from ~3.57 to ~4.21 eV at the absorption edge when going from micro- to NP.

Figure 4 depicts the photoluminescence spectra of $Ca_2Y_{6.4}Eu_{1.6}Si_6O_{26-\delta}$ polycrystals and NP at λ_{ex} = 394 nm. The $^5D_0 \rightarrow {}^7F_0$ transition band is inhomogeneously broadened. Its decomposition into Gaussian components allows distinguishing two bands. The Gaussian 1 has λ_{max} = 577.6 nm, and 2 - λ_{max} = 579.9 nm. These bands confirm the existence of two optical centers formed by Eu^{3+}. Since at Y substitution the Eu^{3+} ion occupies two crystallographic positions in the structure of silicate, 4f and 6h, it forms two types of optical centers. The spectrum are the total luminescence spectrum of these two centers. The spectra contain also a broad band with a maximum at 443 nm, for which the Eu^{2+} ions are responsible ($4f^65d \rightarrow 4f^7(^8S_{7/2})$ transition). The mechanism of formation of Eu^{2+} ions can be the following. When $Ca_2Y_{6.4}Eu_{1.6}Si_6O_{26-\delta}$ polycrystals are synthesized by high-temperature annealing of a mixture of initial components, $V_{Ca}^{//}$ vacancies are formed in the 4*f* position of the produced oxyapatite. The $V_{Ca}^{//}$ vacancies give their negative charge to two Eu_Y^{3+} or Eu_{Gd}^{3+} ions. This leads to the formation of Eu^{2+}.

From comparison of the micro- and NP spectra it is seen that the luminescence of the Eu^{3+} ions in the nanophosphors is almost suppressed. The luminescence of the NP is due mainly to the Eu^{2+} ions. The band maximum is at ~448 nm. By decomposing the Eu^{2+} luminescence spectra into Gaussians, it is possible to estimate the luminescence maxima of the two centers formed by Eu^{2+} ions in the 6h and 4f positions in the apatite structure. The Gaussian 1 has λmax = 444.2 and 2 - 472.5 nm. In the luminescence spectrum of Eu^{2+} ions of the nanosample produced by evaporation of $Ca_2Y_{6.4}Eu_{1.6}Si_6O_{26-\delta}$ in vacuum, Gaussian I has λ_{max} = 465.5 nm and Gaussian II − λ_{max} = 543.0 nm. It can be supposed that the Eu^{2+} ions are additionally formed in the nanosamples due to radiation reduction $Eu^{3+} \rightarrow Eu^{2+}$. Such reduction during exposure to ionizing radiation (α, β, γ, X-Ray and laser) is possible in compounds containing SiO_4 groups [17, 18]. The mechanism of this process can be as follows. Electron is released from the SiO_4^{4-} tetrahedron due to Si─O bond rupture during evaporation of the sample by irradiation of pulsed electron beam. The $(SiO_4^{3-})^+$ state emerges [19]. The released electron is captured by Eu^{3+} ions acting as electron-trapping centers [20]; Eu^{3+} is reduced to Eu^{2+}.

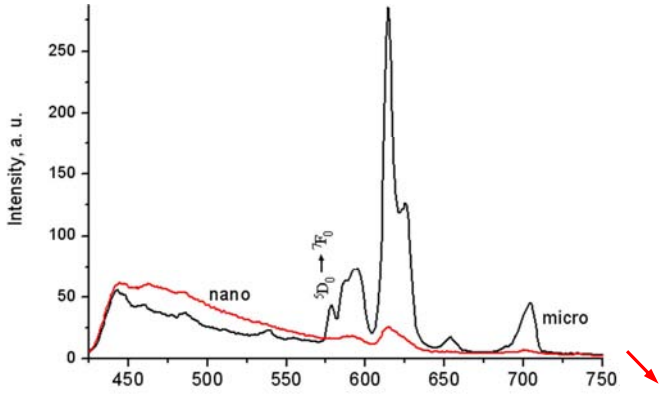

Figure 4. *The photoluminescence spectra of micro- and NP.*

Figure 5 shows the excitation spectra of the samples. A part of the broad band in the λ_{ex} interval 260 – 300 nm is due to the charge transfer process for the Eu^{3+} ions in the microsamples. For the NP, this band is virtually absent, which is indicative of a decrease in the concentration of Eu^{3+} ions. The broad band in the interval 310 – 400 nm is due to the transition of $4f^65d$ ions of Eu^{2+}. For the nanosample the Eu^{2+} excitation spectrum (λ_{em} = 443 nm) is almost the same

as for the bulk sample.

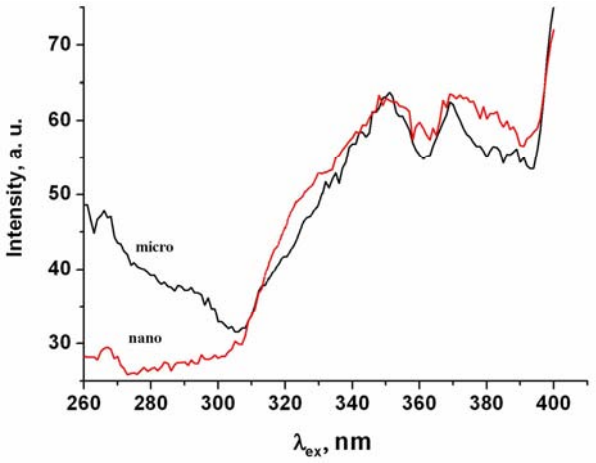

Figure 5. *The excitation spectra of the samples (λ_{em} = 443 nm) of micro- and NP.*

4. Conclusions

Thus, silicate NP in the nanoamorphous state have been produced for the first time from polycrystals of the composition $Ca_2Y_8(SiO_4)_6O_2$: Eu by electron beam evaporation of target. The spectral luminescent characteristics of $Ca_2Y_{6.4}Eu_{1.6}Si_6O_{26-\delta}$ phosphors in polycrystalline state and in nanoamorphous state obtained on the basis of polycrystals have been studied. It was found that the Raman spectrum is modified when the particles decrease from micro- to nanodimensional state. A resonance transfer of excitation energy from the Eu^{3+} ions to the Eu^{2+} ions in micro- and nanophosphors was detected.

Acknowledgements

The authors thank I. V. Baklanova, for help with the recording of Raman-spectra and PL-spectra of the samples.

*A recently published article: M.G. Zuev at al. J. of Luminescence, http://dx.doi.org/10.1016/j.jlumin.2017.04.006

References

[1] M. G. Zuev, S. Yu. Sokovnin, V. G. Il'ves, I. V. Baklanova, A. A. Vasin // J. Solid State Chemistry 218 (2014) 164–170.

[2] A. A. Vasin, M. G. Zuev, E. V. Zabolotskaya, I. V. Baklanova, L. A. Akashev, R. F. Sammigulina // J. Lumin., vol. 168, pp. 26–37, 2015.

[3] V. A. Ishchenko, M. G. Zuev, A. A. Vasin, V. V. Yagodin, L. V. Viktorov, B. V. Shulgin // J. Lumin., vol. 169, Part A, pp. 137–142, 2016.

[4] S. Yu. Sokovnin, V. G. Il'ves1, M. G. Zuev // Chapter 2. Production of complex metal oxide nanopowders using pulsed electron beam in low-pressure gas for biomaterials application in book «Engineering of Nanobiomaterials Applications of Nanobiomaterials» vol. 2, pp. 29–76, 2016.

[5] M. G. Zuev, A. M. Karpov, A. S. Shkvarin // J. Solid State Chem., vol. 184, pp. 52-58, 2011.

[6] A. M. Karpov, M. G. Zuev // Glass Physics and Chem., vol. 38, pp. 431-436, 2012.

[7] R. El. Ouenzerfi, C. Goutaudier, M. Th. Cohen-Adad at al. // J. Lumin., vol. 102–103, pp. 426-433, 2003.

[8] L. Boyer, B. Piriou, J. Carpena, J. L. Lacout. // J. Alloys Compd., vol. 311, pp. 143-152, 2000.

[9] F. Flory, L. Escoubas, G. Berginc // J. Nanophotonics, vol. 5, pp. 052502-052502, 2011.

[10] Nanophotonics-foresight-report-june-2011. Report eds. N. van Hulst, S. Kennedy. ICFO-The Institute of Photonic Sci. Barcelona, Spain. www.nanophotonic-foresight- report-june-2011.

[11] S. Yu. Sokovnin, V. G. Il'ves, M. G. Zuev. Production of complex metal oxide nanopouders using pulsed electron beam in low-pressure gas for biomaieriats application. Chapter 2 in Engineering of Nanobiomaterials Applications of Nanobiomaterials. Vol. 2. Edited by Alexandru Grumezescu, Elsevier 2016.

[12] S. Brunauer Adsorbtsiya gazov i parov. Tom 1. Fizicheskaya adsorbtsiya (The adsorption of gases and vapors. Vol. 1. Physical adsorption). Moscow: Izdatinlit, 1948. 781 p.

[13] Yu. K. Voron'ko, A. A. Sobol', V. E. Shukshin, A. I. Zagumennyi, Yu. D. Zavartsev, S. A. Kutovoi, Physics of the solid state 54 (2012) 1635-1642.

[14] A. N. Lazarev, A. P. Mirgorodskii, I. S. Ignat'ev, Vibrational Spectra of Complex Oxides, Nauka, Leningrad (1975) 296 ([in Russian]).

[15] C. Y. Xu, P. X. Zhang, L. Yan // J. Raman Spectrosc., vol. 32, pp. 862-865, 2001.

[16] K. Rout, M. Mohapatra, S. Anand // Applied Surface Science, vol. 270, pp. 205-218, 2013.

[17] Manveer Singh, P. D. Sahare, Pratik Kumar, Shaila Bahl, Columbia International Publishing, J. of Luminescence and Applications 3 (2016) 1-10.

[18] E. Malchukova, B. Boizot, Materials Research Bulletin 45 (2010) 1299-1303.

[19] A. F. Zatsepin, A. I. Kukharenko, V. A. Pustovarov, V. Yu. Yakovlev, and S. O. Cholakh, Physics of the Solid State 51 (2009) 465-473.

[20] Ryosuke Yokota, J. Phys. Soc. Jpn. 23 (1967) 129-130.